Islamic Azad University

Journal of
Optoelectronical Nanostructures

Autumn 2021 / Vol. 6, No. 4

Research Paper

Design of NIR-TERS System Based on Optimized Grating on the AFM Probe Under Radial Polarized Light for Detection of Molecular Sample

Mohsen Katebi Jahromi[1], Rahim Ghayour[*,1], Zahra Adelpour[1]

[1] Department of Electrical Engineering, Shiraz Branch, Islamic Azad University, Shiraz, Iran.

Received: 10 Sep. 2021
Revised: 5 Oct. 2021
Accepted: 20 Nov. 2021
Published: 15 Dec. 2021

Use your device to scan and read the article online

Keywords:
AFM, NIR Sensor, Plasmon, Spectroscopy, TERS.

Abstract

To the best of our knowledge, it is for the first time that TERS system in near-infrared (NIR) spectrum is reporting. The current study proposed a most favorable atomic force microscopy (AFM) tip based on an incorporated optimal grating structure close to the tip apex. The optimized M^2 factor and the best spatial resolution are obtained as 5.9×10^9 and 8.5 nm respectively in the NIR range of radiation light. The results show that the optimized grating can effectively increase the amount of intensity of electric field and improve spatial resolution within the nanoslit between the AFM tip and substrate. The detection sensitivity of materials can be done by our proposed AFM-TERS system. The difference between the maximum enhancement factors that are correlated to several under test sample molecules show the selectivity potential of the proposed AFM-TERS system in material detection topic.

Citation: Katebi Jahromi M, Ghayour R, Adelpour Z, Design of NIR-TERS system based on optimized grating on the AFM probe under radial polarized light for detection of molecular sample.
Journal of Optoelectronical Nanostructures, 2021; 6 (4): 1- 20.
DOI: 10.30495/JOPN.2022.28490.1228

***Corresponding author:** Rahim Ghayour
Address: Department of Electrical Engineering, Shiraz Branch, Islamic Azad University, Shiraz, Iran. **Tell:** 0098917055393, **Email:** rghayour@shirazu.ac.ir

1. INTRODUCTION

In the past twenty years, TERS has attracted enormous consideration owing to its nanometric spatial resolution and single molecule sensing [1]. This technique has been utilized in many fields of research, such as biological examinations [2], photovoltaics [3], semiconductors [4], carbon nanotubes [5], graphene [6], and detection of single molecules [7]. Raman signal needs to be enhanced through using a novel approach [8]. One of these approaches is integrating the AFM and the Raman spectroscopy in a system set. Fig.1 shows the principle of TERS schematically. A sharp metallic tip which can be considered as an optical antenna is irradiated by the laser beam, leading to a powerfully nanoscale focused electric field close to the apex of tip [9,10], that is confined and boosted because of the combination of three mechanisms as; the gap mode resonance, localized surface plasmon resonance (LSPR) and lightning rod effect.

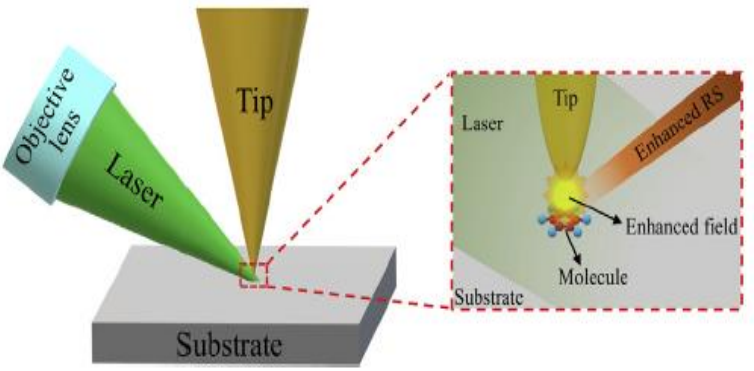

Fig. 1. The schematic of the AFM-TERS principle [11].

Both the surface plasmons and the lightning-rod effect are the local features of nanoscope structures having dimensions that are less than the incident light wavelengths, where it is related to the generation of optical near-fields [9]. The lightning-rod effect is a non-resonant feature of sharp interfaces between materials of differing refractive indices [12].

It is possible to detect much greater enhancement factors in a nanoscale slit between two metals [13, 14], where the electric field is increased by capacitive coupling between the metals [15].

In this study, the three-dimensional finite difference time domain (3D-FDTD) method is utilized to solve Maxwell's equations [16]. Implementation the grating

on the Au and Ag tips with optimized structure that is purposed in [17] has been used to improve the intensity of electric field and spatial resolution within the nanogap in the middle of the AFM tip and the substrate. The particle swarm optimization (PSO) algorithm has been applied for TERS system optimization. The PSO algorithm is an effective technique inspired by motion of bird flocks [18,19]. The system is started with a population of accidental solutions, and the exploration for the optimal solution is done by updating descendant [20].

The structure of the paper is as follows. After stating the subject and its importance, in the second part the simulation conditions and computational methods are presented. The grating structure and design method are explained in section 3. In section 4, based on the analysis of the simulation results, the best configuration for TERS system is obtained and the outcomes of the simulations are compared with the results of previously published papers. In the fifth section of the paper the proposed structure is used for detection of biomolecules and finally the conclusion of the paper is given.

2. METHOD AND STRUCTURE

In this paper, for measuring the electromagnetic field strength throughout the space of a defined problem, FDTD method is used. This method is a numerical analysis abased on discretization of differential form of Maxwell equations in the desired volume and period of time [21]. perfectly matched layers are placed all around the simulation area. The spatial mesh size is considered 0.25 nm and simulation time step was $\nabla t = 1.9 \times 10^{-18}$ s. Fig. 2 demonstrates the configuration of the system utilized in this paper. The AFM tip is modeled as an inverse cone with the base diameter of D, length of L, and the cone angle of α.

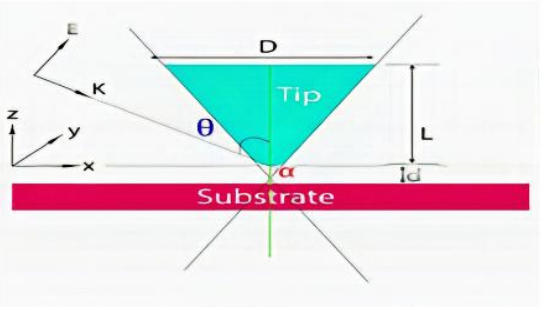

Fig. 2. The AFM tip and gold substrate geometry [22].

A total field scattered field (TFSF) light source that is provide a particular case of plane wave is employed in our simulations to avoid probable coupling to the borders of the simulation region [23]. The laser beam is comprised of a radially polarized light with an electric field of 1.0V/m amplitude. A radially polarized light according to the Richards-Wolf vector diffraction theory is applied [24, 25]. Therefore, in this approach, the focal longitudinal electric field (E_z) and the focal transversal electric field (E_r) can be presented by the underneath equations [26]:

$$E_z=2iA_0 \int_0^{\alpha} P(\theta)\ \mathrm{Cos}^{1/2}\theta\ \mathrm{Sin}^2\theta\ J_0(kr\ \mathrm{Sin}\theta)\exp(ikz\ \mathrm{Cos}\theta)d\theta \quad (1)$$

$$E_r=A_0 \int_0^{\alpha} P(\theta)\ \mathrm{Cos}^{1/2}\theta\ \mathrm{Sin}(2\theta)\ J_1(kr\ \mathrm{Sin}\theta)\ \exp(ikz\mathrm{Cos}\theta)d\theta \quad (2)$$

In the above equations, A_0 is a constant, $k = 2\pi/\lambda$ is the wave vector, α is the maximum focusing angle, J_0 and J_1 are the first type of Bessel function with the orders of 0 and 1, P (θ) is the pupil function of a Bessel Gaussian beam [27]. By solving equations 1 and 2 the focused radially polarized light inside the simulation area is calculated.
The optical constants and parameters of Au and Ag are obtained from [28]. The enhancement factor (EF) of electric field is displayed by M^2 and defined by the following equation [26]:

$$M^2=EF=\left|E_{loc}\right|^2 \Big/ \left|E_0\right|^2 \quad (3)$$

In the above equation $|E_{loc}|$ is the strength of localized electric field close to the tip apex and $|E_0|$ is the strength of the incident light.

3. IMPLEMENTATION OF GRATING

The structure of the TERS system that is used in the simulation of this work is shown in Fig. 3. As it can be seen, the side illumination is used, because by using this configuration, it is possible to achieve a higher M^2 factor compared to other states of radiation like bottom illumination.

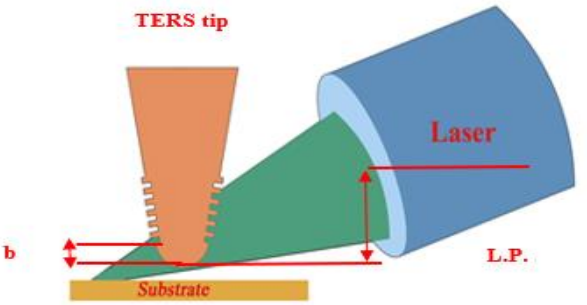

Fig. 3. Proposed AFM-TERS system with gold substrate.

A novel approach for increasing the M^2 factor is implemented a grating structure on the AFM tip. The period, depth and duty cycle of grating and also the direction angle of incident laser light are crucial factors to optimize the system to have the maximum of M^2 factor. As displayed in Fig. 4 The rectangular form is used for modeling the grating.

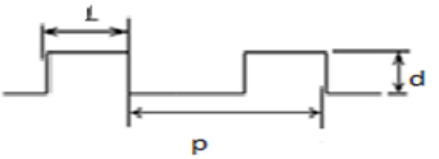

Fig. 4. The model of grating on the AFM tip.

The electric field underneath the tip apex using the formalism of the Green's function can be represented as follows [26]:

$$E(b)=E_0(b)+E_1 e^{i\varphi_1}+E_2 e^{i\varphi_2}+\ldots \quad (4)$$

where $E_0(b)$ is the electric field caused by the tip apex and reliant on b, which is demonstrated in Fig. 3. As for the tip without grating, $E_{total} = E_0$ (b=infinity). other parts of equation 4 are the electric fields produced by the grating grooves with a primary phase of φ_j, depends on the parameters of grating. The first phase φ_j is specified by the optical path of SPPs and the phase delay at the (j–1) th groove. The primary phase φ_j can be presented as [26]:

$$\varphi_{j=}k_{sp}[b+\sum(j-1)(P-L)]/\cos(\alpha/2)+\sum(j-1)\varphi(L) \quad (5)$$

In the above equation k_{sp} is the wave vector of SPPs, φ (L) is the phase lag due to grating grooves. L is the width of grating groove and P is the grating period, both are shown in Fig4. Therefore, the enhancement factor of the electric field increases with the increase in the number of grating grooves, however, the groove number is set at six in further simulations because of considering the fabrication process [17].

The optimized AFM-TERS parameters given in Table 1 (that are obtained by PSO algorithm in [17] by our group) are applied for implementing grating on the AFM tip.

TABLE 1
Results of optimization of different parameters in AFM-TERS system with Au and Ag tips in different steps by PSO algorithm [17]

Material / Optimized Parameters & (Induced field(v/m))	Au tip	Ag tip
Cone angle (α)	20°	5°
Grating distance (b)	1476.5 nm (26.34)	1000 nm (646)
Gratting period (p)	200 nm (37)	159.36 nm (646.5)
Gratting depth (d)	30 nm (49)	30 nm (1030)
Duty cycle (L/P)	0.51 (60)	0.33 (1030)
Laser position (L.P.)	1656.38 nm (232)	1907 nm (1053)
particle distance (P.D.)	2.66 nm (325)	2.66 nm (1433)
Incident angle (θ)	56.2° (5744.5)	50.7° (9899.4)
M^2	3.3×10^7	9.8×10^7

4. SIMULATION RESULTS AND DISCUSSION

In this section, at first the effect of using radially polarized light on the M^2 factor and spatial resolution of the TERS system with conventional (without grating) tip is investigated. Then the optimized AFM-TERS parameters given in Table 1 are applied for implementing grating on the AFM tip. Afterwards, the effects of using gold substrate and radiation on both sides of the tip are inspected in the range of NIR spectrum of laser source.

4.1 The effect of using radially polarized light

If the Au and Ag tips without grating be set in front of the radially polarized light, we can achieve a stronger TERS signal compared to when linearly polarized light is used. Fig. 5 (a) shows the spectral responses M^2 factors for Au and Ag tips of the cone angle of 30° with tip radius of 10 nm under radially polarized light. Based on the simulation results which are reported in [17], the maximum values of electric field enhancement factors are 5182.24 and 9601.6 for Au and Ag tips respectively. These results are obtained using the system without substrate and grating while linearly polarized light perpendicular to the cone axis (θ=90°) is applied. In fact, as demonstrated in Fig.5 (a), the maximum values of M^2 factors are 1.7×10^4 and 2.2×10^4 for Au and Ag tips under radially polarized light (θ=90°). Thus, under the same condition, when the radially polarized light is used instead of the linearly polarized light, the maximum intensity of electrical field becomes much higher, because the longitudinal component of electric field that excite the plasmons is stronger in the radially polarized light. The spatial resolution is another parameter that affects the performance of the AFM-TERS system.

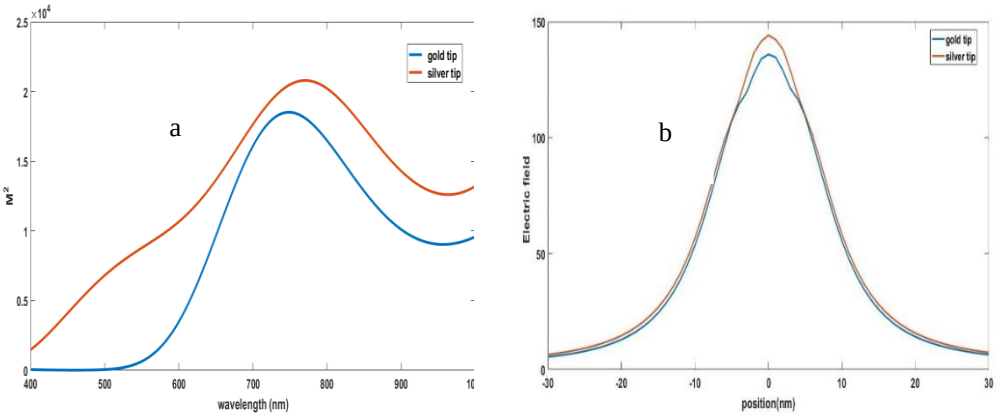

Fig. 5 (a) M^2 factors for the Au and Ag tips with cone angles of 30° under radially polarized light, (b) distributions of electric field at the apex of tips along the x-axis.

In fact, spatial resolution is the full width at half-maximum (FWHM) of the electric field distribution along the x- axis at the resonance wavelength of spectral response of M^2 factor. According to the electric field distribution along x-axis plotted in Fig.5 (b), the spatial resolutions are 19 nm and 17 nm for Au and Ag tips respectively.

In this subsection, based on parameters given in table 1, the spectral responses of M^2 factor for Au and Ag tips in optimal condition under radially polarized light are obtained and demonstrated in Fig. 6 (a). As shown in table 1 the maximum values of M^2 factors are 3.3×10^7 and 9.8×10^7 for Au and Ag tips under linearly polarized light. Meanwhile, as depicted in Fig. 6 (a) the amounts of maximum M^2 factors are 0.52×10^8 and 1.6×10^8 in the range of NIR spectrum of incident light for Au and Ag tips under radially polarized light. Therefore, applying all optimized parameters the M^2 factor of radially polarized light enhanced compared to that of the previous outcomes.

As shown in Fig. 6 (b) the spatial resolution is 12.2 nm and 11.5 nm for Au and Ag tips with grating in optimal conditions under radially polarized light respectively. This is because a more confined hot spot with a higher intensity and smaller size can be created under the tip apex.

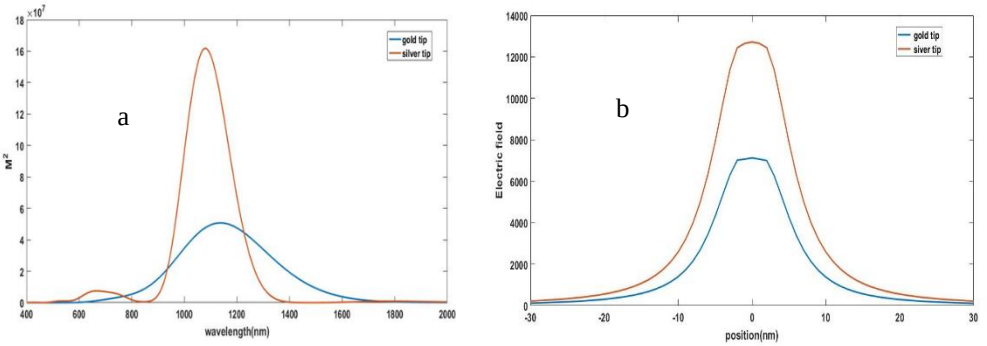

Fig. 6 (a) M^2 factors for the Au and Ag tips with grating under radially polarized light, (b) distributions of electric field at the apex of tips along the x-axis.

In addition to improvement in M^2 factor and spatial resolution, comparing Fig. 5 (a) and 6 (a) reveals that the grating on AFM tips has shifted the resonance wavelengths of the spectral responses from 779.4 nm to 1134.7 nm and 780.7 nm to 1077.4 nm for Au and Ag tips respectively. According to Fig. 5 (a) the bandwidth of spectral response is about 380 nm for the Ag tip without grating, whereas as shown in Fig. 6 (a) for the same Ag tip with grating it is about 200nm. Narrow bandwidth of spectral response of M^2 factor can be useful for next generation application of the TERS system as a biosensor.

It should be mentioned that the spectral responses vary by the geometrical parameters of the grating structure. Generally, the localized surface plasmons are excited if the exciting laser wavelength is equal to the oscillation wavelength of the generated plasmons [29]. On the other hand, the grating parameters especially its duty cycle and the interval between the first groove and the tip apex affect the oscillation wavelength of the generated plasmons and induced electric field at the AFM tip, consequently. According to Fig. 6 (a) the resonant wavelength is in the range of NIR spectrum. Thus, we propose NIR-TERS for the first time that can attract robust interest due to its deep imaging depth, lower band of frequency, narrow spectral bandwidth, and low background interference.

4.2. The effect of using gold substrate

In this section the effect of using substrate on the electric field enhancement factor of AFM-TERS system is investigated carefully. A gold substrate with thickness of 50 nm is placed beneath the tip of AFM-TERS system. Fig.7 (a) demonstrates the spectral responses of the M^2 factors within the nanogap between the gold substrate and the AFM tips, while we applied all the parameters indicated in table1 and under radially polarized light. For the AFM-TERS system including a gold substrate, the enhancement factors are obtained as 1.2×10^8 and 2.02×10^8 for the Au and Ag tips, respectively. Therefore, use of substrate in the proposed AFM-TERS system has a very good efficacy on increasing the amounts of M^2 factor. As shown in Fig.7 (b) the spatial resolutions are 9.5 nm and 8.5 nm for Au and Ag tips respectively. Therefore, use of substrate also improves the spatial resolution to some extent.

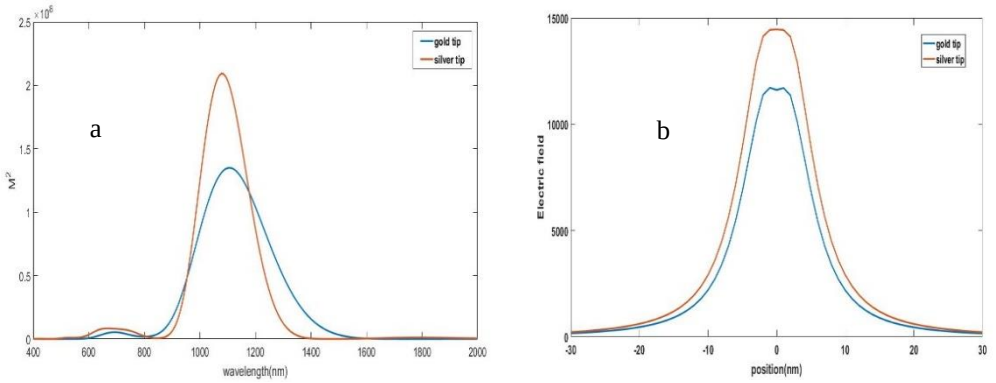

Fig. 7 (a) M^2 factors within the nanogap between the AFM tips and substrate and under radially polarized light in the wavelength range of 400 to 2000 nm of laser source, (b) distributions of electric field within the nanogap between the AFM tips and substrate along the x-axis.

Fig.8 (a) and Fig. 8 (c) demonstrate the distribution of electric fields for the optimized Au and Ag tips with gold substrate respectively. The schemes of field vectors are demonstrated in Fig. 8 (b) and Fig. 8 (d) for Au and Ag tips respectively, where the biggest vectors are focused at the apexes of the Au and Ag tips that confirming the presence of the most powerful electric fields.

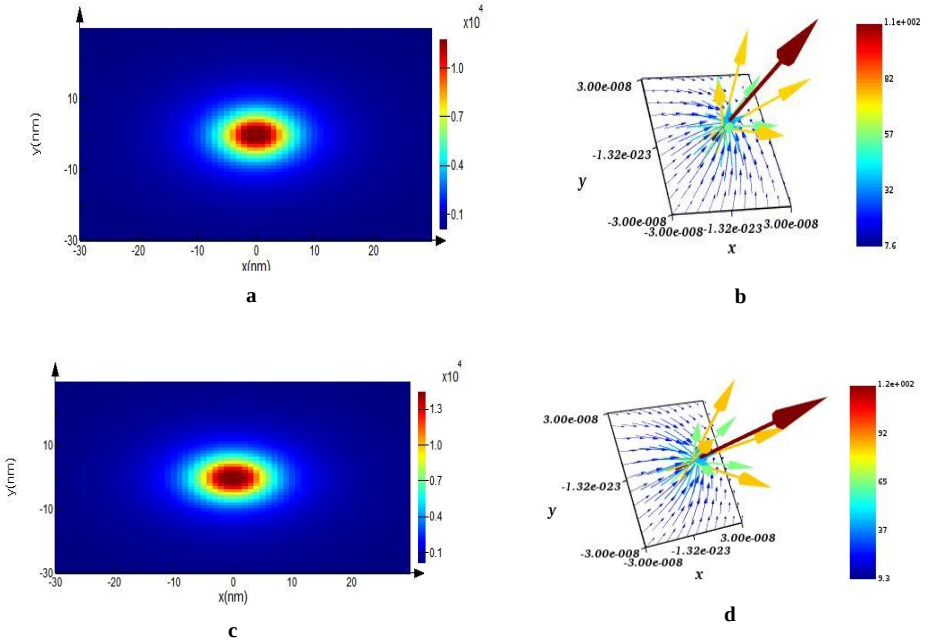

Fig. 8(a), (c) Electric field distributions within the nanogap between the gold substrate and Au and Ag tips respectively and under radially polarized light. (b), (d) Vectors of electric field around the apex of Au and Ag tips with gold substrate respectively.

4.3. The effect of using two laser sources and gold substrate

Now, according to Fig. 9, both sides of the optimal AFM tip are illuminated by two laser sources. The gold substrate is used and radially polarized light is chosen for both lasers. The position and angle of the second source with respect to the tip are the same as those of the first laser but on the opposite side. For the system of Fig. 9, the spectral responses of M^2 factor for the Au and Ag tips are depicted in Fig. 10 (a). Fig.10 (b) demonstrates the electric field distributions along x-axis within the nanogap between the gold substrate and AFM tips in optimal condition under radially polarized light using two laser sources.

By comparing the outcomes of Fig.7 (a) and Fig. 10 (a), it becomes clear that applying the proposed modifications has a considerable efficacy on the optimized M^2 factors as they increased from 1.02×10^8 to 3.65×10^9 and 2.2×10^8 to 5.9×10^9, respectively, in the range of NIR spectrum of incident light. Using two lasers is definitely more effective because the grating on the other side of the tip participates in increasing the electric field at the apex of the Au and Ag tips.

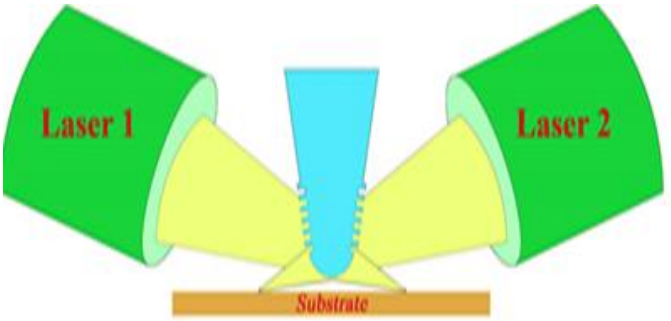

Fig. 9. Both sides of the AFM-TERS system with a gold substrate are illuminated under by two radially polarized lights.

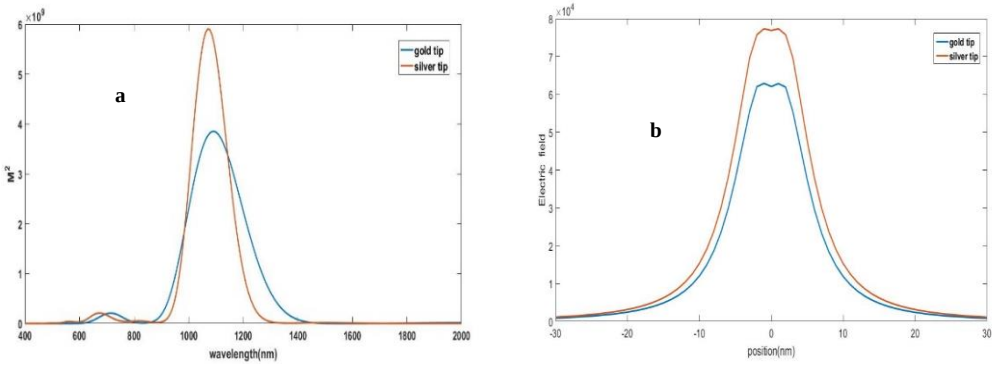

Fig. 10 (a) M^2 factors for the optimal gold and silver tips under radially polarized lights of two laser sources with gold substrate, (b) distributions of electric field within the nanogap between the AFM tips and substrate along the x-axis using two laser sources.

As shown in Fig. 10 (b) compared with the previous cases the spatial resolution is not changed when using two laser sources. Therefore, using two laser sources cannot affect the spatial resolution of the AFM-TERS system, because the mode

confinement of the surface plasmons is not changed in this method.

Fig. 11 (a) and Fig. 11 (c) demonstrate the electric field distributions for Au and Ag tips with gold substrate in optimal condition under radially polarized light using two laser sources, respectively. The schemes of electric field vectors are demonstrated in Fig.11 (b) and 11 (d) for Au and Ag tips, respectively. As Figs. show, the biggest electric field vectors are focused at the apex of the Au and Ag tips, confirming the presence of the most powerful electric fields.

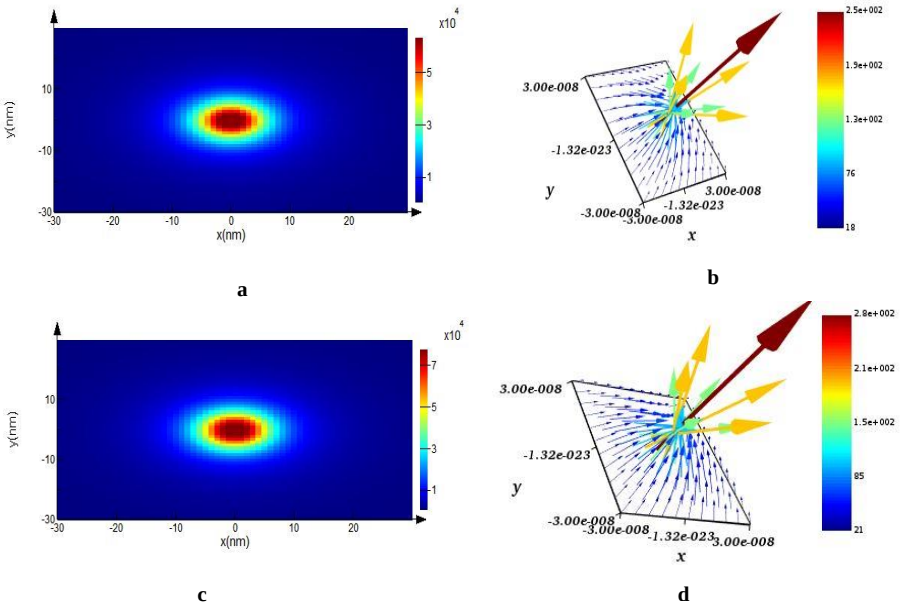

Fig. 11 (a), (c) Electric field distributions for Au and Ag tips with gold substrate under radially polarized light using two laser sources respectively; (b), (d) vectors of electric field around the apex for the optimal Au and Ag tips with gold substrate using two laser sources respectively.

In Table 2 we compared the outcome of this paper with the results reported in other works. As can be seen, in the best conditions, the M^2 factors presented in other works are 3.6×10^7, 1.15×10^4, 1.5×10^4 and 2.8×10^4 in the range of visible spectrum of laser source. Meanwhile, using the proposed method in this paper, the maximum M^2 factor obtained as high as 5.9×10^9 under optimal conditions in

TABLE 2
Comparison of the M^2 factor and wavelength range of our proposed method with those of other works

Refrences	[8]	[23]	[26]	[30]	This paper
Maximum of enhancement factor (M^2)	3.6×10^7	1.15×10^4	1.5×10^4	2.8×10^4	5.9×10^9
The range of wavelength of laser sourcce	200 nm to 500 nm	532 nm	600 nm to 800 nm	400 nm to 800nm	400 nm to 2000 nm

the range of NIR spectrum of incident light.

In addition, comparing the results of this paper with those of the previous study of this group in [17], shows that implementing grating with optimized structure, using gold substrate and radially laser beam have remarkable effect on the electric field intensity of the TERS system. In this paper, for the best condition the spatial resolution is obtained as small as 8.5 nm.

The outcomes of simulations indicate that the electric field at the tip apex in the proposed nanostructure increases sharply compared with that of [31]. This is leading to the generation of hot spot at the tip apex, which, is promising to be used as optical tweezers, where a high-focus laser beam is used to create gravity or repulsive force.

5. DETECTION OF BIOMOLECULES BY NIR-TERS SYSTEM

Now, the optimized silver tip is used for detection of three samples molecules of glucose, hemoglobin and urea. The optical constants of sample material are taken from [32-34]. The molecule of each case is modeled by a sphere with a radius of 10 nanometers and is placed on the substrate. Spectral responses of M^2 factors by the optimized Ag tip with gold substrate for the above-mentioned samples are displayed in Fig. 12. As seen in Fig. 12 the enhancement factor is equal to 5.9×10^9 when there is no particle on the substrate. This is while for sample materials of glucose, hemoglobin and urea they are 9.6×10^9, 10.9×10^9 and 11.8×10^9, respectively. Thus, the enhancement factors of electric field are different for several sample materials. Therefore, the proposed designed TERS

system can effectively discriminated different materials that can be promising as an accurate biosensor for biological application.

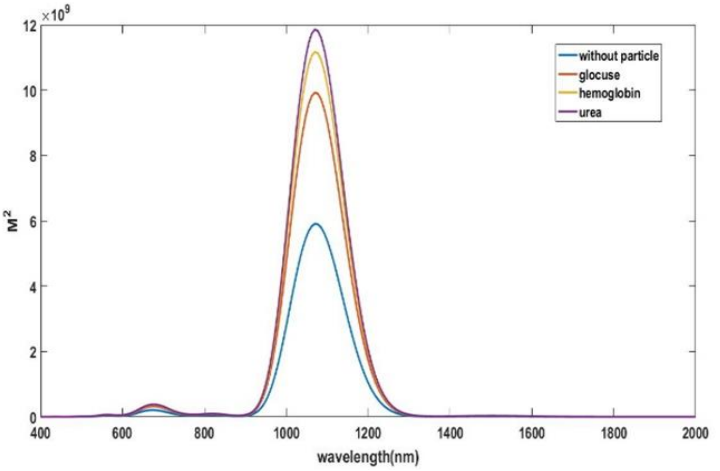

Fig. 12. M^2 factors for the optimized Ag tip with gold substrate for samples of glucose, hemoglobin, urea molecules and without particle in the range of 400 to 2000 nm.

6. CONCLUSION

In this paper, we demonstrated that applying the optimized grating structure on the nanoprobe and using gold substrate under tip apex increase the intensity of electric field and improve the spatial resolution of the TERS system effectively. Moreover, it is presented for the first time that using the approach of this paper, the system can be used in the NIR range of radiation light efficiently, whereas the conventional TERS systems operating in the visible spectrum of electromagnetic wave. In fact, the benefits of infrared imaging have made NIR-TERS a promising approach to overcome the limitations of the conventional (visible) TERS system. Simulation outcomes show that the radially polarized light has a significant effect on the enhancement factor of electric field at the tip apex, compared with that of linearly illumination.

The capability of our proposed AFM-TERS system for detecting the types of materials is examined by placing three sample of molecules as: glucose, hemoglobin and urea on the gold substrate. The differences between the maximum enhancement factors that are obtained for several sample molecules in the study show sensible discrimination of different materials from each other can be realized.

Finally, it is confident that the results of this paper can help fabrication of a

new kind of plasmonic tip for improving the operation of the TERS system in optical microscopy and can be used as a biosensor and optical tweezers as new applications of TERS system.

REFERENCES

[1] J F. Lu, T. Huang, L. Han, H. Su, H. Wang, M. Liu, W. Zhang, X. Wang, T. Mei, *Tip-Enhanced Raman Spectroscopy with High-Order Fiber Vector Beam Excitation*. Sensors (Basel). 18, (2018) 3841. Available: https://dx.doi.org/10.3390%2Fs18113841

[2] S. Najjar, D. Talaga, L. Schue, Y. Coffinier, S. Szunerits, R. Boukherroub, L. servant, V. Rodriguez, S. Bonhommeau, *Tip-enhanced Raman spectroscopy of combed double-stranded DNA bundles*. J. Phys. Chem. C. 118, (2014) 1174–1181. Available: https://www. doi.org/10.1021/jp410963z

[3] X. Wang, D. Zhang, K. Braun, H. J. Egelhaaf, C. J. Brabec, A. J. Meixner, *High-resolution spectroscopic mapping of the chemical contrast from nanometer domains in P3HT: PCBM organic blend films for solar-cell applications*. Adv. Funct. Mater. 20, (2010) 492–499. Available:https://doi.org/10.1002/adfm.200901930

[4] N. Lee, R. D. Hartschuh, D. Mehtani, A. Kisliuk, J. F. Maguire, M. Green, M. D. Foster, A. P. Sokolov, *High contrast scanning nano-Raman spectroscopy of silicon*. J. Raman Spectrosc. 38, (2007) 789–796. Available:10.1002/jrs.1698

[5] Y. Okuno, Y. Saito, S. Kawata, P. Verma. *Tip-enhanced Raman investigation of extremely localized semiconductor-to-metal transition of a carbon nanotube*. Phys. Rev. Lett. 111, (2013) 216101. Available:10.1103/PhysRevLett.111.216101

[6] W. Su, D. Roy, *Visualizing graphene edges using tip-enhanced Raman spectroscopy*. J. Vac. Sci. Technol B. 31, (2013) 041808. Available: https://doi.org/10.1116/1.4813848

[7] R. Zhang, Y. Zhang, Z. C. Dong, S. Jiang, C. Zhang, L. G. Chen, L. Zhang, Y. Liao, J. Aizpurua, Y. Luo, J. L. Yang, J. G. Hou. *Chemical mapping of a single molecule by Plasmon enhanced Raman scattering*. Nature. 498, (2013) 82–86. Available: https://doi.org/10.1038/nature12151

[8] C. Gao, W. Lin, J. Wang, R. Wang, J. Wang. *Principle and Application of Tip-enhanced Raman Scattering*. Plasmonics. 13, (2018) 1343-1358. Available:10.1007/s11468-017-0638-6

[9] M. Rezvani, M. Fathi Sepahvand, *Simulation of Surface Plasmon Excitation in a Plasmonic Nano-Wire Using Surface Integral Equations*, Journal of Optoelectronical Nanostructures, 1(1), (2016), 51-64. Available:20.1001.1.24237361.2019.4.4.5.9

[10] M. Olyaee, M. Bagher Tavakoli, A. Mokhtari, *Propose, Analysis and Simulation of an All Optical Full Adder Based on Plasmonic Waves using Metal-Insulator-Metal Waveguide Structure*, Journal of Optoelectronical Nanostructures, 4 (3), (2019), 95-116.
Available: 20.1001.1.24237361.2019.4.3.7.9

[11] R. Petry, N. C. Oliveira, A. C. Alves, A. G. S. Filho, D. S. T. Martinez, G. Hwang, F. A. Sousa, A. J. Paula, *Chapter 2-Nanomaterials Properties of Environmental Interest and How to Assess Them*. Nanomaterials Applications for Environmental Matrices, Elsevier, (2019) 45-105. Available: https://doi.org/10.1016/B978-0-12-814829-7.00002-1

[12] A. V. Ermushev, B. V. Mchedlishvili, V. A.Oleĭnikov, A. V. Petukhov, *Surface Enhancement of Local Optical Fields and the Lightning-Rod Effect*. Quantum Elec. 23, (1993), 435–440.
Available: https://doi.org/10.1070/QE1993v023n05ABEH003090

[13] S. Y. Ding, E. M. You, Z. Q. Tian, M. Moskovits, *Electromagnetic theories of surface-enhanced Raman spectroscopy*. Chem. Soc. Rev. 46(13), (2017) 4042-76. Available: https://doi.org/10.1039/C7CS00238F

[14] M. M. Sartin, H. S. Su, X. Wang, B. Rena, *Tip-enhanced Raman spectroscopy for nanoscale probing of dynamic chemical systems*. J. Phys Chem. 153, (2020)170901-19. Available: https://doi.org/10.1063/5.0027917

[15] K. Bosnick, M. Maillard, J. Jiang, L. Brus. *Single Molecule Raman Spectroscopy at the Junctions of Large Ag Nanocrystals*. J. Phys. Chem. B. 107(37), (2003) 9964-9972. Available: https://doi.org/10.1021/jp034632u

[16] V. Fallahi, M. Seifouri, *Novel structure of optical add/drop filters and multi-channel filter based on photonic crystal for using in optical*

telecommunication devices. Journal of Optoelectronical Nanostructures, 4(2) (2019) 53-68. Available: 20.1001.1.24237361.2019.4.2.5.

[17] M. Katebi Jahromi, R. Ghayour, Z. Adelpour, *Modeling electric field increment in the Tip-Enhanced Raman Spectroscopy by using grating on the probe of atomic force nanoscope.* Opt Quantum Electron. 53, (2021) 385. Available: http://doi.org/10.1007/s11082-021-03051-2

[18] M. Akhlaghi, F. Emami, *Fuzzy Adaptive Modified PSO-Algorithm Assisted to Design of Photonic Crystal Fiber Raman Amplifier*, Korean J. Opt. Photon, 17, (2013) 237-241. Available: https://doi.org/10.3807/JOSK.2013.17.3.237

[19] A. Asrar, M. Yasrebi, *Application of Classical Bird Swarm Learning Algorithm as a Method of Optimization in Nanotechnology Systems.* Journal of Optoelectronical Nanostructures, 2021; 6(1): 103-126. Available: 10.30495/jopn.2021.4543

[20] F. Emami, M. Akhlaghi, *Gain ripple decrement of S-band raman amplifiers.* IEEE Photon. Technol. Lett, 24, (2012) 1349 -1352. Available: https://doi.org/10.1109/LPT.2012.2203591

[21] Richards, E. Wolf, *Electromagnetic diffraction in optical systems. II. Structure of the image field in an aplanatic system*. Proc. Royal soc A: Math Phys. 253, (1959) 358–379. Available: https://doi.org/10.1098/rspa.1959.0200

[22] Z. Yang, J. Aizpurua, X. Hongxing, *Electromagnetic field enhancement in TERS configurations*, J. Raman. Spectrosc, 40, (2009) 1343–1348. Available: http://dx.doi.org/10.1002/jrs.2429

[23] N. Kazemi-Zanjani, S. Vedraine, F. Lagugné-Labarthet, *Localized enhancement of electric field in tip enhanced Raman spectroscopy using radially and linearly polarized light*. Opt. Express. 21(2013), 25271–25276. Available: https://doi.org/10.1364/OE.21.025271

[24] Q. Zhan, *Cylindrical vector beams: from mathematical concepts to applications.* Adv. Opt. Photonics. 1, (2009) 1-57. Available: https://doi.org/10.1364/AOP.1.000001

[25] B. Richards, E. Wolf, *Electromagnetic diffraction in optical systems. II. Structure of the image field in an aplanatic system*. Proc. Royal soc A: Math Phys. 253, (1959) 358–379.
Available: https://doi.org/10.1098/rspa.1959.0200

[26] F. Lu, W. Zhang, J. Zhang M. Liu, L. Zhang, T. Xue, C. Meng, F. Gao, T. Mei, J. Zhao, *Grating-assisted coupling enhancing plasmonic tip nanofocusing illuminated via radial vector beam*, Nanophotonics. 8, (2019) 2303–2311. Available: https://doi.org/10.1515/nanoph-2019-0329

[27] K. S. Youngworth, T. G. Brown, *Focusing of high numerical aperture cylindrical-vector beams*, opt Express. 7, (2000) 77–87.
Available: https://doi.org/10.1364/OE.7.000077

[28] P. B. Johnson, R. W. Christy, *Optical constants of the noble metals*. Phys Rev B. 6, (1972), 4370-4379.https://doi.org/10.1103/PhysRevB.6.4370

[29] Hamed Azimi, Seyyed Hamid Ahmadi, Mohammad Reza Manafi, Syed Hossein Hashemi Moosavi, Mostafa Najafi, *Development a simple and sensitive method for determination low trace of nickel by local surface plasmon resonance of citrate capped silver nanoparticles*, Journal of Optoelectronical Nanostructures, 6(2) (2021), 23-40.
Available: 20.1001.1.24237361.2021.6.2.1.5

[30] L. Y. Meng, T. Huang, X. Wang, S. Chen, Z. Yang, B. Ren, *Gold-coated AFM tips for tip enhanced Raman spectroscopy: theoretical calculation and experimental demonstration*. Opt. Express, 23, (2015) 13804–13813.
Available: https://doi.org/10.1364/OE.23.013804

[31] L. Long, J. Chen, H. Yu, Z. Y. Li, *Strong optical force of a molecule enabled by the plasmonic nanogap hot spot in a tip-enhanced Raman spectroscopy system*. Photonic Res. 8, (2020) 1573-1579.
Available: https://doi.org/10.1364/PRJ.398243

[32] J. Gienger, K. Smuda, R. Müller, M. Bar, J. Neukammer, *Refractive index of human red blood cells between 290 nm and 1100 nm determined by optical extinction measurements*. Sci. Rep. 9(1), (2019), 4623. Available: https://doi.org/10.1038/s41598-019-38767-5

[33] E. N. Lazareva, V. V. Tuchin, *Measurement of refractive index of hemoglobin in the visible/NIR spectral range*. J. Biomed. Opt. 23(3), (2018)

0350041 -9. Available: https://doi.org/10.1117/1.JBO.23.3.035004

[34] J. R. Warren, J. A. Gordon, *On the Refractive Indices of Aqueous Solutions of Urea*. J. Phys. Chem. 1, (1966) 297–300. Available: https://doi.org/10.1021/j100873a507